Effect of maghemite nanoparticles on insulin amyloid fibril formation: Selective labeling, kinetics, and fibril removal by a magnetic field

Hadas Skaat,[1] Mirco Sorci,[2] Georges Belfort,[2] Shlomo Margel[1]

[1]*Department of Chemistry, Bar-Ilan University, Ramat-Gan 52900, Israel*
[2]*Howard P. Isermann Department of Chemical & Biological Engineering and Center for Biotechnology a Interdisciplinary Studies, Rensselaer Polytechnic Institute, Troy 12180, New York*

Abstract: Maghemite (γ-Fe$_2$O$_3$) magnetic nanoparticles of 15.0 $\pm$ 2.1 nm were formed by nucleation followed by controlled growth of maghemite thin films on gelatin-iron oxide nuclei. Human insulin amyloid fibrils were formed by incubating the monomeric insulin dissolved in aqueous continuous phase at pH 1.6 and 65°C. Magnetic human insulin amyloid fibrils/γ-Fe$_2$O$_3$ nanoparticle assemblies were prepared by interacting the γ-Fe$_2$O$_3$ nanoparticles with the insulin amyloid fibrils during or after their formation. The nanoparticles attached selectively to the insulin fibrils in both cases. The kinetics of the insulin fibrillation process in the absence and the presence of the γ-Fe$_2$O$_3$ nanoparticles was elucidated. The insulin amyloid fibrils/γ-Fe$_2$O$_3$ nanoparticle assemblies were easily extracted from the aqueous phase via a magnetic field. We hypothesize that this selective extraction approach may also be applicable for the removal of other amyloidogenic proteins that lead to neurodegenerative diseases (e.g., Alzheimer's, Parkinson's, Huntington's, mad cow, and prion diseases) from their continuous phase, e.g. milk, blood, neurological fluid, etc. © 2008 Wiley Periodicals, Inc. J Biomed Mater Res 91A: 342–351, 2009

Key words: magnetic nanoparticles; γ-Fe$_2$O$_3$ nanoparticles; insulin amyloid fibrils; protein folding; neurodegenerative diseases

INTRODUCTION

Human diseases characterized by insoluble extracellular deposits of proteins have been recognized for almost two centuries.[1] Amyloidoses have traditionally been defined as diseases in which normally soluble proteins accumulate in the extracellular space of various tissues as insoluble deposits of about 10 nm diameter fibrils.[2] These amyloid fibrils commonly consist of polypeptide chains organized mainly into cross β-sheets, in which the peptide strands are arranged perpendicularly to the long axis of the fibril.[1–8] The formation of amyloid aggregates in tissues is a pathological feature of many neurodegenerative diseases such as Alzheimer's, Parkinson's, Huntington's, mad cow, and prion diseases. There are many examples of secreted circulating proteins that can, under abnormal circumstances, be converted in part to highly stable extracellular fibrils. These include immunoglobulins in primary systemic amyloidosis, multiple myeloma, amylin in the diabetic pancreas and small soluble proteins of uncertain function such as amyloid β-peptide (Aβ) in Alzheimer's disease.[1] However, the mechanism for normal and soluble proteins to assemble into fibrillar and insoluble aggregates still remains unresolved.

In this study, insulin was chosen as a model amyloidogenic protein. The formation of insulin fibrils is a physical process in which non-native (or unfolded) insulin molecules interact with each other to form structure aggregates. Amyloid fibril deposits of insulin had been observed both in patients with type II diabetes as well as after insulin infusion and repeated injection.[1,3] Insulin fibrils are known to deposit in arterial walls and membrane surfaces. Insulin aggregation is a major problem in production, storage, and delivery of the protein.

Recent literature concerning novel biomaterials indicates increasing interest in developing nanoparticles to detect, prevent and treat protein-misfolding diseases.[9–12] Their potential to influence protein fibrillation is a function of both the nanoparticle surface interfacial properties including charge and its enormous surface area/volume. Various nanoparticles such as copolymer particles of *N*-isopropylacrylamide/*N-tert*-butylacrylamide, cerium oxide, quantum dots, and carbon nanotubes have been reported to promote protein assembly into amyloid fibrils *in vitro* by assisting the nucleation process.[13] Metal nanoparticles such as gold or Pd have also been used for metallization of a synthesized peptide fibrils prepared from 12 amino acids residues.[14,15]

Magnetic iron oxide nanoparticles have a large number of potential applications due to their high surface area/volume, magnetic properties, nontoxicity, and biodegradability. These nanoparticles have already been used for the separation of the particles and/or their conjugates from undesired compounds via high gradient magnetic field (HGMF) separation. In addition, they have been used for magnetic recording, magnetic sealing, electromagnetic shielding, and various biomedical uses such as magnetic resonance imaging (MRI), hyperthermia for tumor treatment, cell labeling and sorting, DNA separation and drug delivery.[16–29]

The present article describes a method for specific magnetization of human insulin fibrils by maghemite nanoparticles. γ-Fe$_2$O$_3$ nanoparticles of narrow size distribution were synthesized by nucleation, followed by controlled growth of maghemite thin films onto gelatin-iron oxide nuclei. Human insulin amyloid fibrils were formed by incubating the monomeric insulin dissolved in aqueous continuous phase at pH 1.6 and 65°C. Magnetic human insulin amyloid fibrils/γ-Fe$_2$O$_3$ nanoparticle assemblies were prepared by interacting the γ-Fe$_2$O$_3$ nanoparticles with the insulin amyloid fibrils during or after their formation.[27,28] The nanoparticles were attached selectively to the insulin fibrils in both cases. The kinetics of the insulin fibrillation process in the absence and the presence of the γ-Fe$_2$O$_3$ nanoparticles was determined. In contrast to previous work which indicated that various nanoparticles are used as catalysts for the protein fibrillation process, the γ-Fe$_2$O$_3$ nanoparticles did not significantly affect the lag time and hence the kinetics of nucleation and oligomer formation prior to the formation of the fibrils.[13]

Strategies for extraction of amyloid fibrils from liquid phases have been recently reviewed.[30–33] For example, the removal of abnormal prions from blood and plasma components for increasing the safety profile of plasma products has been reported.[34–40] The present article describes a novel method to remove insulin fibrils from the aqueous phase by binding of the γ-Fe$_2$O$_3$ nanoparticles to the fibrils directly. The formed amyloid fibrils/γ-Fe$_2$O$_3$ nanoparticle assemblies were then completely removed from the aqueous phase by a magnetic field. We hypothesize that this approach may also be applicable for the removal of prion and other amyloidogenic fibrils from their continuous phase, e.g. milk, blood, neurological fluid, etc. This will, of course, depend on the ability of the nanoparticles to bind to these fibrils in complex protein-containing solutions.

MATERIALS AND METHODS

Materials

The following analytical-grade chemicals were purchased from commercial sources and were used without further purification: ferrous chloride tetrahydrate, hydrochloric acid (1*M*), sodium hydroxide (1*M* standard solution), sodium chloride, sodium nitrite, phosphate buffered saline (PBS, 0.1*M*), gelatin from porcine skin, human serum albumin (HSA), and human insulin from Sigma; Mica from Asylum Research, Santa Barbara, CA; water was purified by passing deionized water through an Elgastat Spectrum reverse osmosis system (Elga, High Wycombe, UK).

Synthesis of the γ-Fe$_2$O$_3$ nanoparticles

γ-Fe$_2$O$_3$ magnetic nanoparticles of 15.0 $\pm$ 2.1 nm diameter were prepared according to previous manuscripts.[27,28] Briefly, 240 mg of gelatin was dissolved in 80 mL of water at 60°C. Then, 160 μL of Fe^{+2} solution (10 mmol in 5 mL 0.1 *N* HCl) and 57.6 μL of sodium nitrite solution (7.27 mmol in 5 mL H$_2$O) were added, respectively, to the shaken gelatin solution. For nucleation, titration with sodium hydroxide (1*M*) was then performed until a pH of 9.5 was reached. This procedure was repeated successively four more times. Then, the reaction mixture was shaken at 60°C for an additional 1 h. The formed magnetic γ-Fe$_2$O$_3$ nanoparticles were then washed from nonmagnetic waste with water by the HGMF technique.[27]

Behavior of the γ-Fe$_2$O$_3$ nanoparticles in acidic pH and high temperature

The temperature of a vial containing 10 mL of γ-Fe$_2$O$_3$ nanoparticles (4 mg/mL) dispersed in 0.025*M* HCl aqueous solution containing 0.1*M* NaCl (pH 1.6) was raised from room temperature to 65°C. Samples (0.1 mL) were then taken from the nanoparticles mixture at various time intervals for measuring the diameter and diameter distribution.

Preparation of the human insulin amyloid fibrils

Several tubes each containing 2 mg of human insulin dissolved in 1 mL of 0.025*M* HCl aqueous solution con-

taining 0.1M NaCl (pH 1.6) were incubated at room temperature. For initiating the insulin fibrillation process, the temperature of the insulin solutions was quickly raised to 65°C. Studies of fibrillation kinetics were accomplished by decreasing the temperature of a chosen tube to room temperature at each time interval. All the insulin samples were freshly prepared immediately prior to each experiment in order to minimize the possible formation of fibril nuclei in the solution, which would affect the kinetics of the fibril formation. The concentration of the dissolved monomer and other oligomers was obtained from the calibration absorbance curve at 280 nm versus a series of insulin concentrations. The absorbance at 280 nm was measured after removal of the insulin fibrils by centrifugation. The kinetics of the insulin fibril formation was obtained using the absorbance at 600 nm.

Preparation of the human insulin amyloid fibrils/γ-Fe$_2$O$_3$ nanoparticle assemblies

Human insulin amyloid fibrils were labeled with different concentrations of the γ-Fe$_2$O$_3$ nanoparticles in two ways: (1) Insulin fibrillation in the presence of the γ-Fe$_2$O$_3$ nanoparticles; (2) Addition of the γ-Fe$_2$O$_3$ nanoparticles to already prepared human insulin amyloid fibrils dispersed in aqueous solution at pH 1.6 or in PBS (pH 7.4) solution. Briefly, for the first method, different volumes,7.5–70 μL, (0.03–0.28 mg or 1.5–14.0 (w/w)%) of the γ-Fe$_2$O$_3$ aqueous dispersion (4 mg/mL) were added to 1 mL aqueous solution at pH 1.6 containing 2 mg insulin, as described above. The formation of fibrils was then initiated by quickly raising the temperature of the aqueous mixture from room temperature to 65°C for different time intervals. For the second method, various volumes (as above) of the γ-Fe$_2$O$_3$ aqueous dispersion (4 mg/mL) were added to the insulin fibrils aqueous dispersion at pH 1.6 or pH 7.4. The mixtures obtained were then incubated at room temperature for 3 h. The aqueous dispersion of the human insulin amyloid fibrils at pH 1.6 was prepared as described above, and at pH 7.4 by extensive dialysis of the insulin fibrils aqueous dispersion at pH 1.6 against PBS.

Characterization

Fourier transform infrared (FTIR) analysis was performed with a spectrophotometer (Bomem, model MB100, Hartman and Braun). The analysis was performed with 13 mm KBr pellets that contained either 2 mg of the insulin fibrils (in the absence or the presence of labeled γ-Fe$_2$O$_3$ nanoparticles) samples and 198 mg KBr, or 0.5 mg γ-Fe$_2$O$_3$ nanoparticles and 199.5 mg KBr. The pellets were scanned over 200 scans at a 4 cm^{-1} resolution.

Transmission electron microscope (TEM) images were obtained with an electron microscope (Model JEOL-JEM 100SX) with 80–100 kV accelerating voltage. High-resolution TEM (HRTEM) images were obtain by employing an accessory (JEOL-3010) to the JEOL-TEM device with 300 kV accelerating voltage. Samples for TEM and HRTEM were prepared by placing a drop of diluted sample on a 400-mesh carbon-coated copper grid. The dry particles' av-

erage size and size distribution were determined by measuring the diameter of more than 100 particles with the image analysis software (AnalySIS Auto, Soft Imaging System GmbH, Germany).

Hydrodynamic diameter and size distribution of the nanoparticles dispersed in aqueous continuous phase were measured using a submicron particle analyzer (Model N4 Plus, Coulter Electronics, England).

Magnetic measurements were performed at room temperature with an Oxford Instrument vibrating sample magnetometer (VSM, oxford Instruments, UK).

Absorbance measurements at 280 and 600 nm were performed with UV–visible spectrophotometer (model Carry-1E, from Varian company, Australia).

Atomic force microscope (AFM) imaging was performed using MFP-3D-SA AFM (Asylum research, Santa Barbara, CA) and standard silicon cantilevers (AC240TS, Olympus America, Center Valley, PA). All experiments were performed in air under ambient conditions. For routine AFM-imaging the tapping mode was employed. Samples for
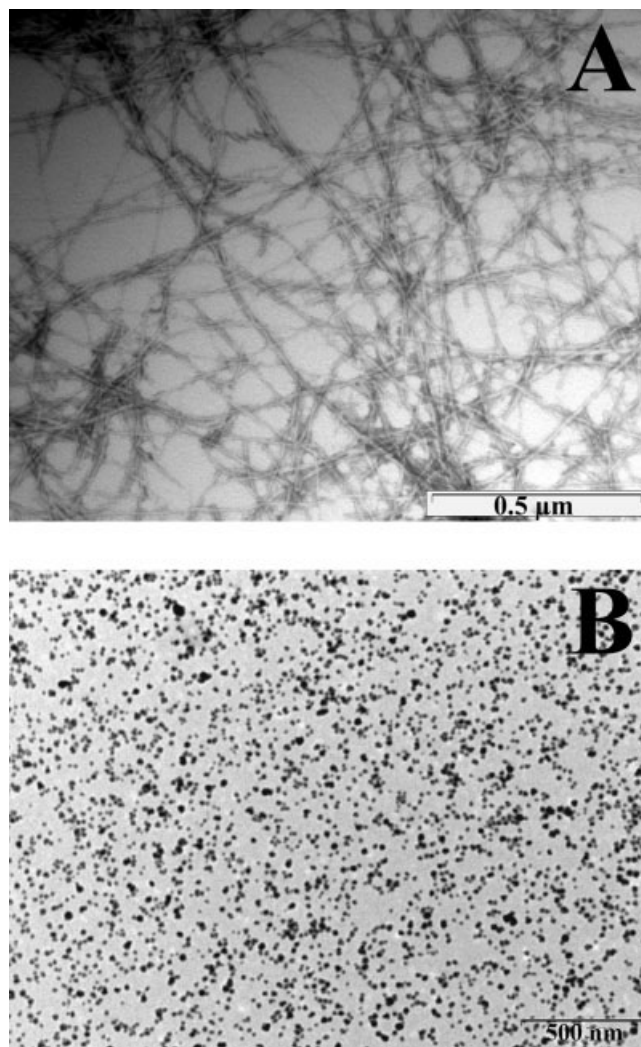
Figure 1. TEM images of the human insulin amyloid fibrils (A) and the γ-Fe$_2$O$_3$ nanoparticles (B). The insulin fibrils and the γ-Fe$_2$O$_3$ nanoparticles were prepared according to the experimental section.
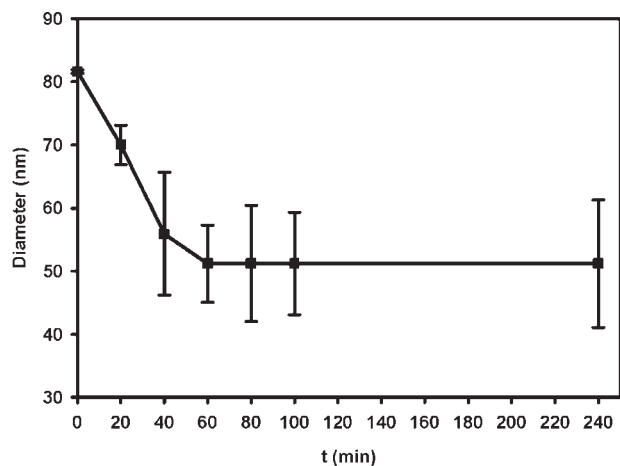
Figure 2. Time-dependent change of the size and size distribution of the γ-Fe$_2$O$_3$ nanoparticles dispersed in aqueous continuous phase at pH 1.6 and 65°C. 0.1 mL samples were taken at various time intervals from 10 mL aqueous dispersion of the γ-Fe$_2$O$_3$ nanoparticles (4 mg/mL) in 0.025M HCl containing 0.1M NaCl (pH 1.6) at 65°C. The hydrodynamic size and size distribution of the nanoparticles were measured according to the experimental section.

AFM were prepared by placing a drop of diluted sample of the insulin fibrils/γ-Fe$_2$O$_3$ nanoparticle assemblies on mica surfaces.

RESULTS AND DISCUSSION

TEM images of the human insulin fibrils and the γ-Fe$_2$O$_3$ nanoparticles are illustrated in Figure 1(A,B), respectively. Figure 1(A) shows the fibrous and nonbranching structure of the insulin fibrils with lengths up to several micrometers and an average diameter of about 10 nm. However, due to the low contrast in the TEM image, the detailed structure of the human insulin fibrils is not completely clear. The TEM image of the γ-Fe$_2$O$_3$ nanoparticles [Fig. 1(B)] demonstrates that these nanoparticles are stable against agglomeration and possess a diameter of 15.0 $\pm$ 1.2 nm. Light scattering measurements performed in our lab show that the diameter and size distribution of the γ-Fe$_2$O$_3$ nanoparticles dispersed in water is 81.6 $\pm$ 0.2 nm. The difference between the diameter of the nanoparticles measured by TEM and light scattering is due to the fact that the first method measures the dry diameter of the nanoparticles while the second one measures the hydrodynamic diameter, which takes into account the surface adsorbed solvent molecules and the swelling of the particles by the solvent molecules.

The change of the hydrodynamic diameter and size distribution of the γ-Fe$_2$O$_3$ nanoparticles with time at pH 1.6 at 65°C is presented in Figure 2. A
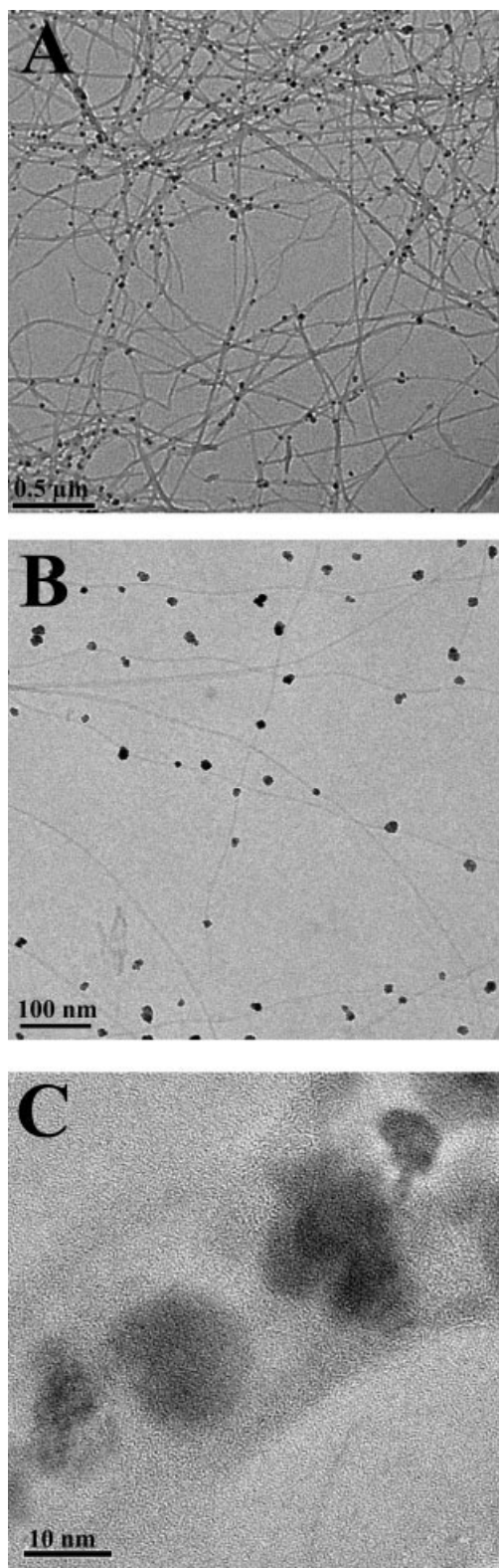
Figure 3. TEM (A), cryo-TEM (B), and HRTEM (C) images of the human insulin fibrils labeled with the γ-Fe$_2$O$_3$ nanoparticles. The insulin fibrils/γ-Fe$_2$O$_3$ nanoparticle assemblies were prepared by adding 1.5 (w/w)% γ-Fe$_2$O$_3$ nanoparticles to 1 mL aqueous solution at pH 1.6 containing 2 mg insulin.
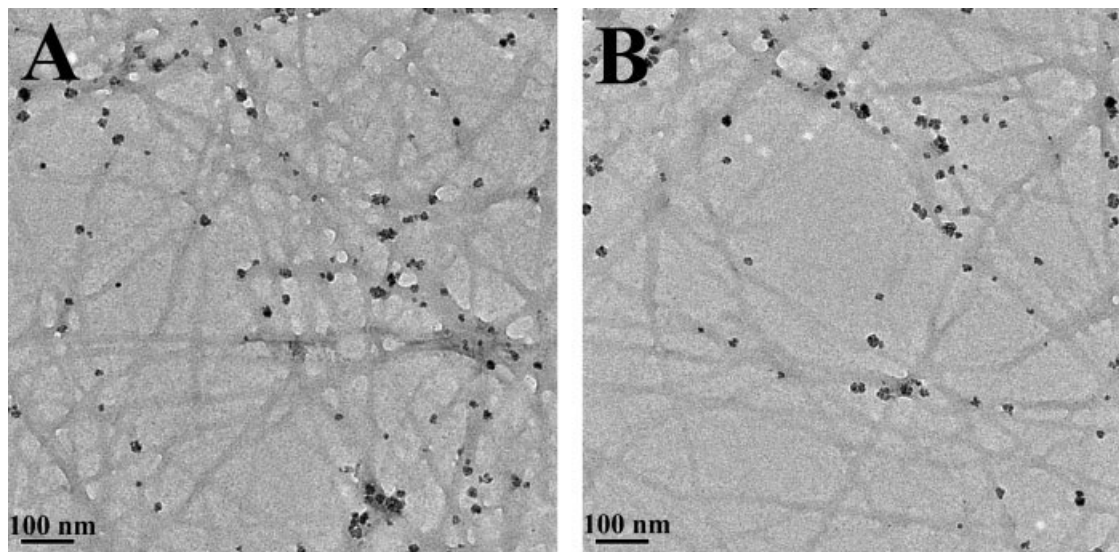
Figure 4. TEM images of the human insulin fibrils/γ-Fe$_2$O$_3$ nanoparticle assemblies prepared by addition of the γ-Fe$_2$O$_3$ nanoparticles to the insulin fibrils dispersed in aqueous continuous phase at pH 1.6 (A) and pH 7.4 (B). 1.5 (w/w)% γ-Fe$_2$O$_3$ nanoparticles were added to 2 mg insulin amyloid fibrils dispersed in 1 mL aqueous solution at pH 1.6 and at pH 7.4 (PBS).

significant increase in the size distribution of the nanoparticles due to the change in the continuous phase from water at room temperature to 0.025M HCl aqueous solution containing 0.1M NaCl (pH 1.6) at 65°C is observed. This figure also illustrates a systematic decrease in the hydrodynamic diameter of the particles during the first 60 min from about 81.6 ± 0.2 nm to 51.2 ± 8.2 nm. Thereafter, up to 240 min, no significant change in the diameter was noticed. However, if the aqueous dispersion of magnetic nanoparticles were stored under these conditions for a few days, complete dissolution of the γ-Fe$_2$O$_3$ in the aqueous phase was observed. Thus, within the time scale of the experiments of several hours the particles were stable.

Data for TEM (A), cryo-TEM (B), and HRTEM (C) images of the human insulin fibrils/γ-Fe$_2$O$_3$ nanoparticle assemblies prepared in the presence of the γ-Fe$_2$O$_3$ nanoparticles, by adding the nanoparticles before the onset of the fibril formation, are presented in Figure 3. The γ-Fe$_2$O$_3$ nanoparticles appear to bind freely with the axial external surface of the fibrils with almost no freely unassociated suspended nanoparticles. Careful measurements indicate that the dry diameter of the γ-Fe$_2$O$_3$ attached to the insulin fibrils is 9.0 ± 1.5 nm. We assume that the decrease of the original diameter of the nanoparticles from 15.0 ± 1.2 to 9.0 ± 1.5 nm is derived from the acidic media of the γ-Fe$_2$O$_3$ nanoparticles, which leads to a gradual decrease in the nanoparticle diameter, as was illustrated in Figure 2. The cryo-TEM image [Fig. 3(B)] reveals that the γ-Fe$_2$O$_3$ nanoparticles are attached to the insulin fibrils in real time and are not due to the water evaporation that is

required for preparing the TEM images. The γ-Fe$_2$O$_3$ nanoparticles self-assemble at the surfaces of the insulin fibrils probably through charge and/or hydrophobic interactions. The HRTEM image [Fig. 3(C)] of individual insulin-γ-Fe$_2$O$_3$ fibril clearly demonstrates the edges of the fibril and the adsorbed nanoparticles on the surface of this fibril. These data illus-
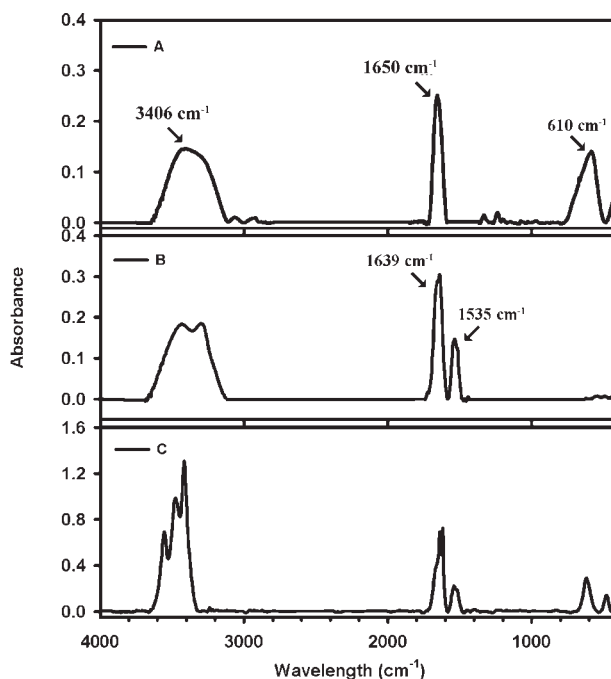
Figure 5. FTIR spectra of the γ-Fe$_2$O$_3$ nanoparticles (A) and insulin fibrils in the absence (B) and the presence (C) of 1.5 (w/w)% γ-Fe$_2$O$_3$ nanoparticles added to the aqueous continuous phase after completion of the fibrillation process.
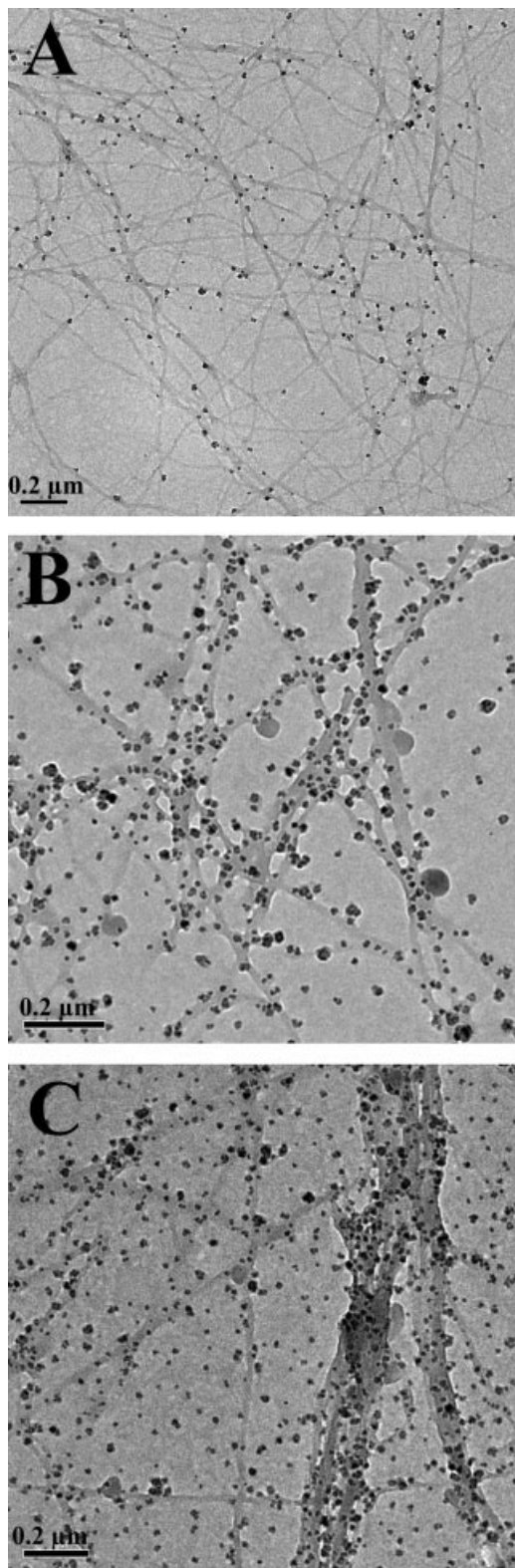
Figure 6. TEM images of the human insulin amyloid fibrils/γ-Fe$_2$O$_3$ nanoparticle assemblies prepared by addition of different concentrations of the γ-Fe$_2$O$_3$ nanoparticles to the insulin fibrils dispersed in aqueous continuous phase at pH 1.6. 1.5 (A), 14.0 (B), and 24.0 (C) (w/w)% γ-Fe$_2$O$_3$ nanoparticles were added to 2 mg insulin amyloid fibrils dispersed in 1 mL aqueous continuous phase at pH 1.6.

trate strong binding of the magnetic nanoparticles to the insulin fibrils during the fibril reaction.

Next, the γ-Fe$_2$O$_3$ nanoparticles were added after completion of the insulin reaction, i.e. post addition. The data shown in Figure 4 at pH 1.6 (A) and at pH 7.4 (B) is similar to those from Figure 3. Nearly all the particles are bound to the fibril external surface while little or none are seen free away from the fibrils. Similar results were also observed under competitive conditions, e.g., in the presence of 4% HSA at pH 7.4.

The FTIR spectra of the γ-Fe$_2$O$_3$ nanoparticles (A) and of the insulin fibrils at pH 1.6 in the absence (B) and presence (C) of 1.5 (w/w)% γ-Fe$_2$O$_3$ nanoparticles (0.03 mg nanoparticles/2 mg insulin fibrils) are shown in Figure 5. For the last case the γ-Fe$_2$O$_3$ nanoparticles were added after the completion of the fibrillation process. The IR spectrum of the γ-Fe$_2$O$_3$ nanoparticles [Fig. 5(A)] shows a typical absorbance peak at 610 cm^{-1} corresponding to the vibration band of Fe—O, a peak at 1650 cm^{-1} corresponds to the gelatin N—H stretching band and a very broad peak at 3406 cm^{-1} belonging to the vibrational band of O—H. The latter peak is probably due to the presence of surface hydroxyl groups (Fe—OH) of the iron oxide and carboxyl groups of the gelatin. The IR spectrum of the insulin fibrils [Fig. 5(B)] shows a peak at 1535 cm^{-1} corresponding to the vibrational band of N—H (amide II), a peak at 1639 cm^{-1} corresponding to the stretching band of C=O (amide I), indicating antiparallel and parallel β-sheets, and peaks at 3299 and 3435 cm^{-1} corresponding to the stretching vibration of N—H. The IR spectrum of the insulin fibrils/γ-Fe$_2$O$_3$ nanoparticle assemblies [Fig.
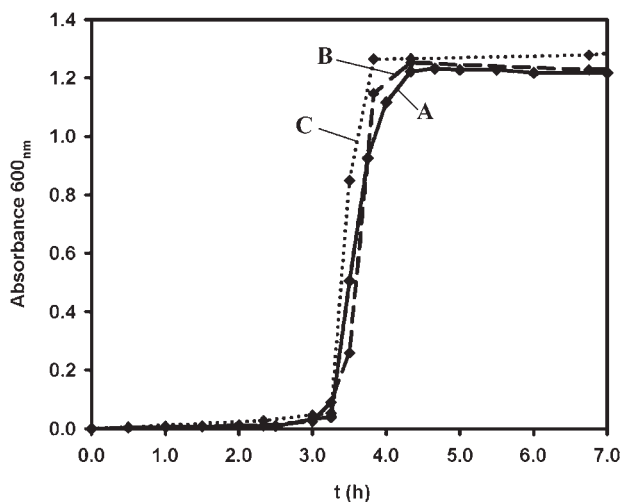
Figure 7. Sigmoidal kinetics of the fibril formation using absorption at 600 nm as a function of time at pH 1.6 in the absence (A) and the presence of 1.5 (B) and 24.0 (C) (w/w)% γ-Fe$_2$O$_3$ nanoparticles. The γ-Fe$_2$O$_3$ nanoparticles were added to 2 mg monomeric insulin dispersed in 1 mL aqueous solution at pH 1.6 and 65°C.
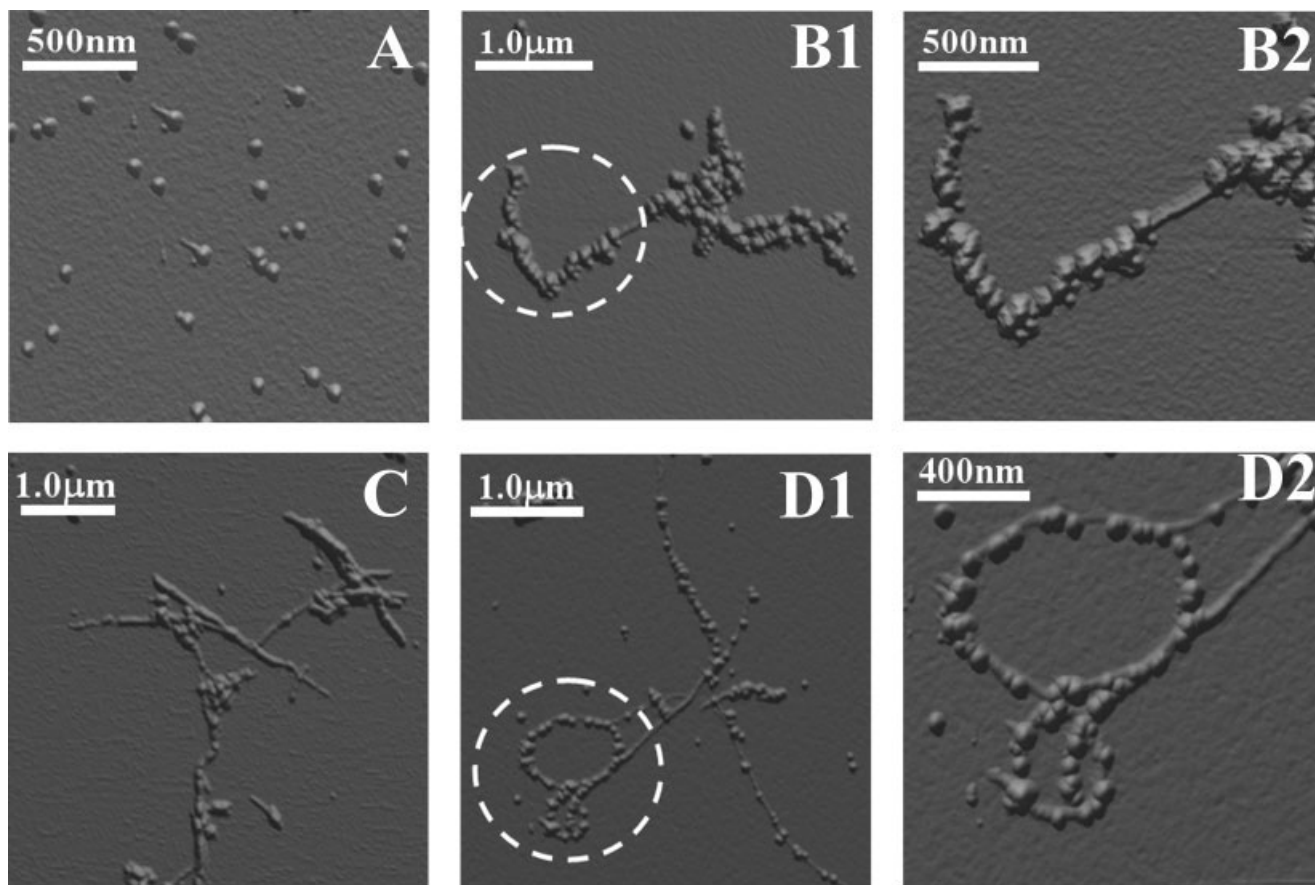
Figure 8. AFM images of the human insulin amyloid fibrils/γ-Fe$_2$O$_3$ nanoparticle assemblies prepared by fibrillation of human insulin in the presence of 6 (w/w)% of γ-Fe$_2$O$_3$ nanoparticles for different time intervals: 3.0 (A), 3.5 (B1,B2), 4 (C) and 5.0 (D1,D2) h. B2 & D2 represent higher magnification of the circled regions shown in B1 and D1, respectively. The γ-Fe$_2$O$_3$ nanoparticles were added to 2 mg human insulin dispersed in 1 mL aqueous solution at pH 1.6 and 65 °C.

5(C)] is composed of peaks belonging both to the insulin fibrils (e.g., 1535 and 1639 cm^{-1}) and to the γ-Fe$_2$O$_3$ nanoparticles (610 and 3406 cm^{-1}), thereby demonstrating the attachment of the γ-Fe$_2$O$_3$ nanoparticles to the insulin fibrils.

TEM photomicrographs in Figure 6 illustrate the interaction between human insulin fibrils prepared at pH 1.6 with increasing concentrations of the γ-Fe$_2$O$_3$ nanoparticles. With increased loading of the γ-Fe$_2$O$_3$ nanoparticles, the amount of nanoparticles bound to the fibrils increases. For example, in the presence of 1.5 (w/w)%, only a relatively small fraction of each fibril is coated [Fig. 6(A)], while at 14.0 (w/w)% nanoparticles the density of the coated particles on the fibrils increases significantly [Fig. 6(B)]. For the highest concentration of the nanoparticles at 24.0 (w/w)% the fibrils are maximally coated and the excess unbound nanoparticles are clearly observed in the background of the TEM image [Fig. 6(C)].

Typical sigmoidal curves for the formation of insulin fibrils at pH 1.6 and 65°C in the absence (A) and the presence of different concentrations [1.5 (B) and 24.0 (C) wt %] of the γ-Fe$_2$O$_3$ nanoparticles are

shown in Figure 7. In the absence or the presence of the nanoparticles a similar behavior was observed: the main growth of the insulin fibrils was initiated
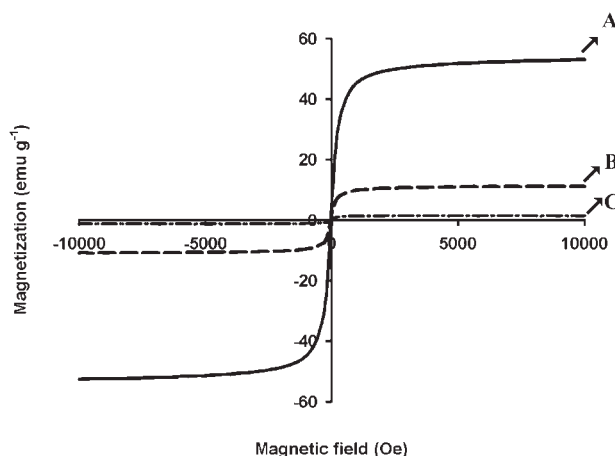
Figure 9. Magnetization curves of the γ-Fe$_2$O$_3$ nanoparticles (A) and human insulin fibrils/γ-Fe$_2$O$_3$ nanoparticle assemblies prepared by addition of 14.0 (B) and 1.5 (C) (w/w)% of γ-Fe$_2$O$_3$ nanoparticles to the insulin fibrils dispersed in aqueous continuous phase at pH 1.6. The γ-Fe$_2$O$_3$ nanoparticles were added to 2 mg insulin amyloid fibrils dispersed in 1 mL aqueous continuous phase at pH 1.6.
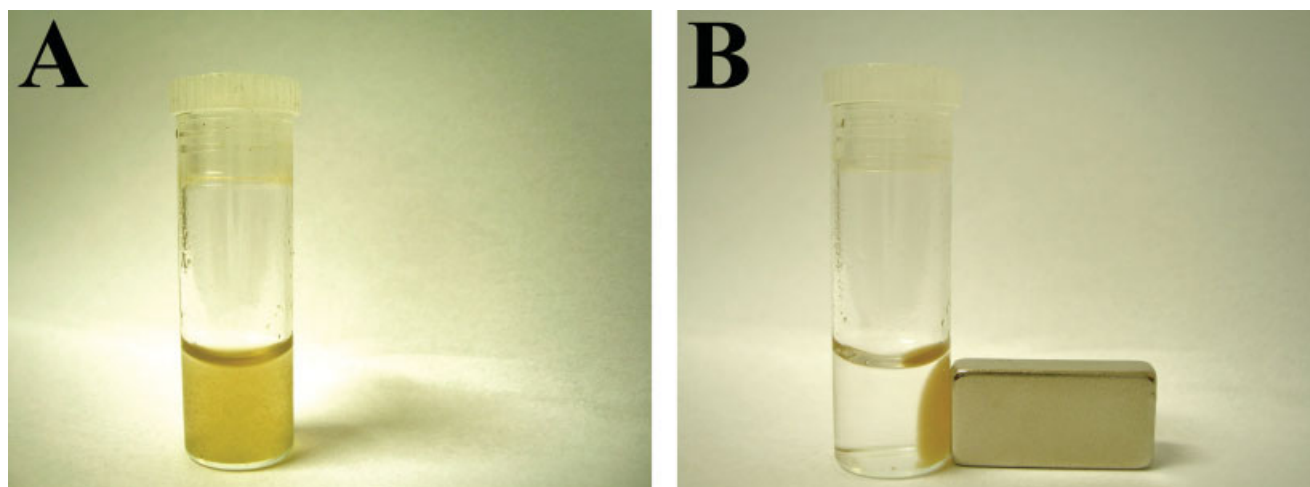
Figure 10. Magnetic insulin amyloid fibrils dispersed in aqueous continuous phase, before (A) and after (B) applying a magnetic field. The insulin fibrils/γ-Fe$_2$O$_3$ nanoparticle assemblies were prepared by addition of 1.5 (w/w)% γ-Fe$_2$O$_3$ nanoparticle to 2 mg insulin amyloid fibrils dispersed in 1 mL aqueous continuous phase at pH 1.6.

~3.0 h after initiating the fibrillation process and completed after ~5.0 h. It should be noted that after removal of the insulin fibrils generated after 4.5 h, the absorbance of the supernatant at 280 nm was zero, indicating that all the monomeric insulin had already been converted to insulin fibrils. This figure also demonstrates that the kinetics of insulin fibril growth appears to be almost unaffected by the presence of the different concentrations of the γ-Fe$_2$O$_3$ nanoparticles.

The AFM images in Figure 8 show the growth kinetics of the human insulin fibrils/ γ-Fe$_2$O$_3$ nanoparticle assemblies for samples taken at 3–5 h during the insulin fibrillation process, see Figure 7(A). Here, the samples were prepared with fresh monomeric insulin dispersed in an aqueous continuous phase at pH 1.6 and 65°C in the presence of 6.0 (w/w)% of the γ-Fe$_2$O$_3$ nanoparticles. The AFM image taken 3.0 h after the initiation of the fibrillation process [Fig. 8(A)] reveals the appearance of small spherical-like aggregate structure, which may indicate the onset of the growth of the fibrils. Figure 8(B–D) illustrates the gradual growth with time of the insulin fibrils. The relatively small fibrils are linear, while the longer ones are partially twisted. Figure 8 also indicates the selective binding the γ-Fe$_2$O$_3$ nanoparticles onto the insulin fibrils, with almost no free nanoparticles in the background.

The magnetization curves at room temperature of the γ-Fe$_2$O$_3$ nanoparticles (A) and the human insulin fibrils/γ-Fe$_2$O$_3$ nanoparticle assemblies prepared by addition of 1.5 (B) and 14.0 (C) weight % γ-Fe$_2$O$_3$ nanoparticles to the insulin fibrils dispersed in aqueous continuous phase at pH 1.6 are shown in Figure 9. It is readily observed that the M(H) curve of the

γ-Fe$_2$O$_3$ nanoparticles has no hysteresis loop. Zero field cooled-field cooled (ZFC-FC) measurements of the γ-Fe$_2$O$_3$ nanoparticles exhibit blocking temperature (T_B) at ca. 275 K, which indicate a superparamagnetic behavior.[41] Figure 9 also illustrates that all the M(H) plots reach saturation at fields of around 2000 Oe. The staturation magnetization of the γ-Fe$_2$O$_3$ nanoparticles [Fig. 9(A)] is 58 emu/g while the labeled fibrils with 14.0 and 1.5 (w/w)% of the γ-Fe$_2$O$_3$ nanoparticles [Fig. 9(B,C), respectively] are 11.3 and 1.42 emu/g, respectively. The difference in the magnetization of the labeled fibrils is probably related to the different concentrations of the γ-Fe$_2$O$_3$ nanoparticles attached to the fibrils. The higher the concentration the higher is the saturation magnetization.

A relatively simple and convenient way to remove the insulin amyloid fibrils from the aqueous continuous phase is shown in Figure 10. Advantage is taken of the binding of the γ-Fe$_2$O$_3$ nanoparticles to the insulin fibrils. The magnetic insulin amyloid fibril assemblies are easily removed from the aqueous phase using a simple magnet. Scale up of this process, assuming that the particles will adhere to the fibrils under competitive adsorption conditions (i.e in complex solutions like cereable fluid or fermentation broth), should not be too complicated.

CONCLUSIONS

In Summary, this article describes the synthesis and characterization of magnetic human insulin amyloid fibrils/γ-Fe$_2$O$_3$ nanoparticle assemblies, by

selective binding of γ-Fe_2O_3 nanoparticles to human insulin fibrils. The kinetics of the insulin fibrillation process in the absence and the presence of the γ-Fe_2O_3 nanoparticles was also illustrated. The removal of the insulin amyloid fibrils from its continuous phase by magnetization has been illustrated. In future studies we plan to extend the present work to other amyloidogenic proteins, e.g., prions, amyloid β, β_2-microglobulin, etc. under competitive adsorption conditions. In addition, we plan to modify the surface of the magnetic nanoparticles with ligands of different functionality and chemical nature and explore the effect of the various nanoparticles on the kinetics of the protein fibrillation process

References

1. Selkoe DJ. Folding proteins in fatal ways. Nature 2003;426: 900–904.
2. Sunde M, Blake CC. From the globular to the fibrous state: Protein structure and structural conversion in amyloid formation. Q Rev Biophys 1998;31:1–39.
3. Bouchard M, Zurdo J, Nettleton EJ, Dobson CM, Robinson CV. Formation of insulin amyloid fibrils followed by FTIR simultaneously with CD and electron microscopy. Protein Sci 2000;9:1960–1967.
4. Klunk WE, Debnath ML, Koros AMC, Pettegrew JW. Chrysamine-G, a lipophilic analogue of Congo red, inhibits A β-induced toxicity in PC12 cells. Life Sci 1998;63:1807–1814.
5. Klunk WE, Wang YM, Huang GF, Debnath ML, Holt DP, Mathis CA. Uncharged thioflavin-T derivatives bind to amyloid-beta protein with high affinity and readily enter the brain. Life Sci 2001;69:1471–1484.
6. Sethuraman A, Vedantham G, Imoto T, Przybycien T, Belfort G. Protein unfolding at interfaces: Slow dynamics of α-helix to β-sheet transition. Proteins 2004;56:669–678.
7. Sethuraman A, Belfort G. Protein structural perturbation and aggregation on homogeneous surfaces. Biophys J. 2005;88: 1322–1333.
8. Link CD, Johnson CJ, Fonte V, Paupard MC, Hall DH, Styren S, Mathis CA, Klunk WE. Visualization of fibrillar amyloid deposits in living, transgenic Caenorhabditis elegans animals using the sensitive amyloid dye, X-34. Neurobiol Aging 2001; 22:217–226.
9. Kogan MJ, Bastus NG, Amigo R, Grillo-Bosch D, Araya E, Turiel A, Labarta A, Giralt E, Puntes VF. Nanoparticle-mediated local and remote manipulation of protein aggregation. Nano Lett 2006;6:110–115.
10. Cox DL, Lashuel H, Lee KYC, Singh RRP. The materials science of protein aggregation. MRS Bull 2005;30:452–457.
11. Cui ZR, Lockman PR, Atwood CS, Hsu CH, Gupte A, Allen DD, Mumper RJ. Novel D-penicillamine carrying nanoparticles for metal chelation therapy in Alzheimer's and other CNS diseases. Eur J Pharm Biopharm 2005;59:263–272.
12. Ji XJ, Naistat D, Li CQ, Orbulescu J, Leblanc RM. An alternative approach to amyloid fibrils morphology: CdSe/ZnS quantum dots labelled β-amyloid peptide fragments A β (31-35), A β (1-40) and A β (1-42). Colloid Surf B: Biointerfaces 2006;50:104–111.
13. Linse S, Cabaleiro-Lago C, Xue WF, Lynch I, Lindman S, Thulin E, Radford SE, Dawson KA. Nucleation of protein fi-

14. brillation by nanoparticles. Proc Natl Acad Sci USA 2007; 104:8691–8696.
15. Fu XY, Wang Y, Huang LX, Sha YL, Gui LL, Lai LH, Tang YQ. Assemblies of metal nanoparticles and self-assembled peptide fibrils—Formation of double helical and single-chain arrays of metal nanoparticles. Adv Mater 2003;15:902–906.
16. Reches M, Gazit E. Controlled patterning of aligned self-assembled peptide nanotubes. Nat Nanotechnol 2006;1:195–200.
17. Babes L, Denizot B, Tanguy G, Le JJ Jeune, Jallet P. Synthesis of iron oxide nanoparticles used as MRI contrast agents: A parametric study. J Colloid Interface Sci 1999;212:474–482.
18. Kim DK, Zhang Y, Kehr J, Klason T, Bjelke B, Muhammed M. Characterization and MRI study of surfactant-coated superparamagnetic nanoparticles administered into the rat brain. J Magn Magn Mater 2001;225:256–261.
19. Hergt R, Hiergeist R, Hilger I, Kaiser WA, Lapatnikov Y, Margel S, Richter U. Maghemite nanoparticles with very high AC-losses for application in RF-magnetic hyperthermia. J Magn Magn Mater 2004;270:345–357.
20. Pardoe H, Clark PR, Pierre TG St, Moroz P, Jones SK. A magnetic resonance imaging based method for measurement of tissue iron concentration in liver arterially embolized with ferrimagnetic particles designed for magnetic hyperthermia treatment of tumors. Magn Reson Imaging 2003;21:483–488.
21. Chemla YR, Grossman HL, Poon Y, McDermott R, Stevens R, Alper MD, Clarke J. Ultrasensitive magnetic biosensor for homogeneous immunoassay. Proc Natl Acad Sci USA 2000; 97:14268–14272.
22. Uhlen M. Magnetic Separation of DNA. Nature 1989;340:733–734.
23. Debuire B, Chabli A, Frenoy N. Fast, Manual, nonradioactive method for DNA-sequencing. Clin Chem 1993;39:1682–1685.
24. Yoza B, Matsumoto M, Matsunaga T. DNA extraction using modified bacterial magnetic particles in the presence of amino silane compound. J Biotechnol 2002;94:217–224.
25. Scherer F, Anton M, Schillinger U, Henkel J, Bergemann C, Kruger A, Gansbacher B, Plank C. Magnetofection: Enhancing and targeting gene delivery by magnetic force in vitro and in vivo. Gene Ther 2002;9:102–109.
26. Bergemann C, Muller-Schulte D, Oster J, Brassard, LA, Lubbe AS. Magnetic ion-exchange nano- and microparticles for medical, biochemical and molecular biological applications. J Magn Magn Mater 1999;194:45–52.
27. Rudge SR, Kurtz TL, Vessely CR, Catterall LG, Williamson DL. Preparation, characterization, and performance of magnetic iron-carbon composite microparticles for chemotherapy. Biomaterials 2000;21:1411–1420.
28. Margel S, Gura S. Nucleation and growth magnetic metal oxide nanoparticles and its use.WO 996207, 1999.
29. Ziv O, Avtailion R, Margel S. Acquired and natural immiginicity of gelatin, dextran and human serum albumin conjugated to magnetite nanoparticles. J Biomed Mat Res Part A 2008;85:1011–1021.
30. Margel S, Tennenbaum T, Gura S, Tsubery M. Lab Tech Biochem Mol Biol Ed. Amsterdam, The Netherlands: Maciej Zborowski, Elsevier B.V; 2007.
31. Majumdar A, Cruz D, Asamoah N, Buxbaum A, Sohar I, Lobel P, Maxfield FR. Activation of microglia acidifies lysosomes and leads to degradation of Alzheimer amyloid fibrils. Mol Biol Cell 2007;18:1490–1496.
32. Yan P, Hu XY, Song HW, Yin KJ, Bateman RJ, Cirrito JR, Xiao QL, Hsu FF, Turk JW, Xu J, Hsu CY, Holtzman DM, Lee JM. Matrix metalloproteinase-9 degrades amyloid-β fibrils in vitro and compact plaques in situ. J Biol Chem 2006;281:24566–24574.
33. Hirschfield GM, Hawkins PN. Amyloidosis: New strategies for treatment. Int J Biochem Cell Biol 2003;35:1608–1613.

33. Rosenblum WI. Structure and location of amyloid beta peptide chains and arrays in Alzheimer's disease: New findings require reevaluation of the amyloid hypothesis and of tests of the hypothesis. Neurobiol Aging 2002;23:225–230.

34. Flan B, Arrabal S. Manufacture of plasma-derived products in France and measures to prevent the risk of vCJD transmission: Precautionary measures and efficacy of manufacturing processes in prion removal. Transfus Clin Biol 2007;14:51–62.

35. Prowse V. Prion removal with filters. ISBT Sci Ser 2006;1:230–234.

36. Vey M, Baron H, Weimer T, Groner A. Purity of spiking agent affects partitioning of prions in plasma protein purification. Biologicals 2002;30:187–196.

37. Hammond DJ, Lathrop JT, Cervenakova L, Carbonell RG. Prion protein ligands and use in prion protein detection and removal and in treating prion-associated diseases. Application:WO2003US38343, 2004050851, 2004

38. Hammond DJ, Wiltshire VR, Carbonell R. Prion-binding ligands and methods of using same. Application: WO 2001US11150, 2001077687, 2001.

39. Prusiner SB, Safar JG. Removal of prions from blood, plasma and other liquids. Application:US 99-235372, 6221614, 2001.

40. Solomon A, Wall J, Hrncic R, Schell M. Methods of investigating, diagnosing, and treating amyloidosis. Application: WO2001US11043, 2001077167, 2001.

41. Boguslavsky Y, Margel S. Synthesis and characterization of poly(divinylbenzene)-coated magnetic iron oxide nanoparticles as precursor for the formation of air-stable carbon-coated iron crystalline nanoparticles. J Colloid Interface Sci 2008;317:101–114.